Rogue Waves in Higher Order Nonlinear Schrödinger Models

Constance M. Schober[1] and Annalisa Calini[2]

[1] Department of Mathematics, University of Central Florida, Orlando, FL 32816
cschober@mail.ucf.edu
[2] Department of Mathematics, College of Charleston, Charleston, SC 29424
calinia@cofc.edu

Summary. We discuss physical and statistical properties of rogue wave generation in deep water from the perspective of the focusing Nonlinear Schrödinger equation and some of its higher order generalizations. Numerical investigations and analytical arguments based on the inverse spectral theory of the underlying integrable model, perturbation analysis, and statistical methods provide a coherent picture of rogue waves associated with nonlinear focusing events. Homoclinic orbits of unstable solutions of the underlying integrable model are certainly candidates for extreme waves, however for more realistic models such as the modified Dysthe equation two novel features emerge: (a) a chaotic sea state appears to be an important mechanism for both generation and increased likelihood of rogue waves; (b) the extreme waves intermittently emerging from the chaotic background can be correlated with the homoclinic orbits characterized by maximal coalescence of their spatial modes.

1 Introduction

Among the various mechanisms for wave amplification under different physical conditions, the Benjamin-Feir (BF) instability and nonlinear self focusing are often proposed in relation to rogue wave generation in deep water. In particular, the work of Henderson et al, [13] suggests that excitation of certain breather-like solutions of the focusing nonlinear Schr̈odinger (NLS) equation

$$iu_t + u_{xx} + 2|u|^2 u = 0, \tag{1}$$

triggers the formation of rogue waves. Trulsen and Dysthe's analysis [34] of the sea state during the famous New Year Wave event recorded at the North Sea Draupner Platform in 1995 (see Fig. 1) shows a weakly nonlinear wave train with a relatively narrow frequency bandwidth, thus supporting the use of the focusing NLS equation as a basic model for studying rogue waves in deep water.

A stability analysis of solutions of the NLS equation shows that low frequency modes may become unstable and that the number of unstable modes

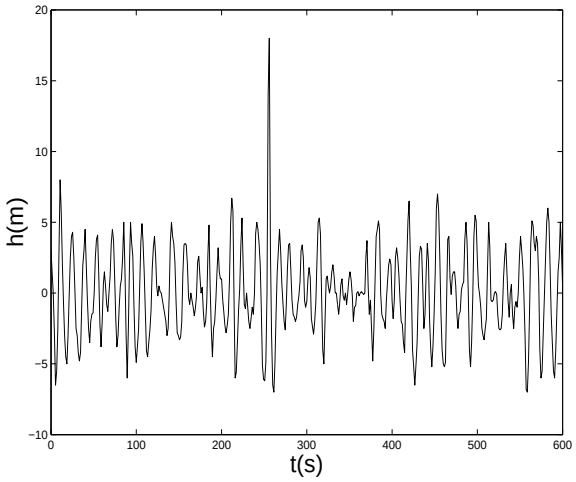

Fig. 1. Time series of the surface elevation of the 1995 New Year Wave Event.

increases with the amplitude of the carrier wave. Homoclinic orbits of unstable NLS solutions, including those of an unstable Stokes wave, exhibit many of the properties observed in rogue waves [28, 9, 17]. However, generic homoclinic orbits of unstable solutions of the NLS equation are unlikely to be physically observable in more realistic models of deep water wave dynamics (for example, those described by higher order generalizations of the NLS equation). It is thus important to develop criteria for rogue wave formation for general sea states, to investigate whether proximity to unstable solutions of the integrable model can be correlated to rogue wave generation, and to determine the robustness of the homoclinic orbits under physically meaningful perturbations.

A more realistic description of deep water wave dynamics is provided by the Modified Dysthe (MD) equation,

$$iu_t + u_{xx} + 2|u|^2u + i\epsilon^{1/2}\left(\frac{1}{2}u_{xxx} - 6|u|^2u_x + u^2u_x^* - 2ui\left[H\left(|u|^2\right)\right]_x\right) + \epsilon\,\frac{5}{16}u_{4x} + i\epsilon^{3/2}\,\frac{7}{32}u_{5x} = 0,$$

introduced by Trulsen and Dysthe [32, 33] by retaining higher order terms in the asymptotic expansion of the surface wave displacement. (Here $H(f)$ denotes the Hilbert transform of the function f.)

Laboratory experiments conducted in conjunction with numerical simulations by the first author and her collaborators [1, 2], established that, for higher order generalizations of the NLS equations, the generic long-time dynamics of initial data near an unstable Stokes wave with two unstable modes is chaotic. Further numerical investigations of the MD equation revealed that for a general class of such initial data, high amplitude coherent structures arise

intermittently above the chaotic background [9]. Remarkably, these emerging coherent structures are structurally similar to maximal homoclinic orbits of the unperturbed Stokes wave with coalesced spatial phases (which are also the homoclinic orbits of maximal amplitude). Such optimally phase modulated homoclinic solutions of the NLS equation appear to be the only homoclinic solutions which persist under perturbations, their persistence being independent of phase selection of the initial conditions [9, 30]. In other words, a chaotic sea state due to proximity to unstable NLS solutions appears to increase the occurrence of rogue waves, enhance focusing effects, and select, among homoclinic solutions, those that are good candidates for modelling physically observable rogue waves.

In order to analyse this phenomenon in more detail, we regard the MD equation as a perturbation of the NLS equation. A combination of tools from the integrable theory of the NLS equation, and a formal extension of the Melnikov method for perturbations of Hamiltonian systems with homoclinic structures are used to address both structural and statistical properties of the observed rogue waves.

In section 2 we review elements of the periodic theory for the integrable NLS equation, the analytical construction of homoclinic solutions (from low-dimensional to maximal homoclinic manifolds) of the unstable Stokes wave, and discuss wave amplification due to phase coalescence, as well as the relation between phase singularities, wave compression, and wave amplification.

In section 3 we study the effects of homoclinic chaos on rogue wave generation, and discuss numerical simulations of the MD equation (8) and its restriction to spatially symmetric wave trains. (See e.g. Fig. 5b.) "Noisy" rogue waves emerge intermittently above a chaotic background: we discuss how the likelihood of rogue wave occurrence as well as wave focusing are found to increase in the chaotic regime.

In section 4 we present a formal Melnikov-type calculation aimed at explaining the persistence of optimally phase modulated homoclinic orbits during the perturbed chaotic dynamics. These persisting coherent structures are thus natural candidates for the physically observable rogue waves.

The remaining sections use a statistical approach (in combination with the periodic theory of the integrable NLS), to develop a criterion for rogue wave prediction, and a statistical description of rogue waves associated with homoclinic chaos in both the NLS and MD models.

In section 5, we discuss rogue wave generation for random sea states characterized by the Joint North Sea Wave Project (JONSWAP) power spectrum. The JONSWAP spectrum was introduced to describe developing sea states with ongoing nonlinear wave-wave interactions [27, 5].) A spectral quantity, the "splitting distance" between simple periodic points of the Floquet spectrum of an initial condition in a neighborhood of an unstable NLS solution, is proposed as a measurement of the proximity in spectral space to unstable waves and homoclinic data. For regimes in which few (two or three) unstable modes are present, hundreds of realizations of JONSWAP type initial data

show that, in both the pure NLS and the MD models, rogue waves develop for small splitting distance, and do not when the splitting distance is large [14].

In the final section a statistical interpretation of rogue waves in both the NLS and MD equations is provided. Using the third and fourth statistical moments of the wave elevation for sea states characterized by JONSWAP spectra with random phases, we examine dependence of skewness, kurtosis, and likelihood of rogue waves on the proximity to unstable waves and homoclinic data. Extensive numerical studies reveal that wave strength, skeweness, and kurtosis all increase as the spectral splitting distance decreases, thus supporting the claim that modulational instability is not only an important mechanism for rogue wave generation, but also a significant source of non-Gaussianity in the water wave statistics. Finally, consistent with the numerical and analytical studies described in the first part of this article, statistically, the NLS equation appears to under predict, as compared to the MD equation, both the strength and likelihood of rogue waves.

2 Background

As is well-known, the nonlinear Schrödinger (NLS) equation is equivalent to the solvability condition of the AKNS system, the pair of first-order linear systems [37]:

$$\mathcal{L}^{(x)}\boldsymbol{\phi} = 0, \qquad \mathcal{L}^{(t)}\boldsymbol{\phi} = 0, \tag{2}$$

for a vector-valued function $\boldsymbol{\phi}$. The linear operators on the left-hand sides of (2) are

$$\mathcal{L}^{(x)} = \begin{pmatrix} \partial_x + i\lambda & -u \\ u^* & \partial_x - i\lambda \end{pmatrix}, \mathcal{L}^{(t)} = \begin{pmatrix} \partial_t + i(2\lambda^2 - |u|^2) & -2\lambda u - iu_x \\ 2\lambda u^* - iu_x^* & \partial_t - i(2\lambda^2 - |u|^2) \end{pmatrix},$$

and depend on x and t through the NLS potential u and on the *spectral parameter* λ.

The nonlinear spectral decomposition of an NLS initial condition (or in general of an ensemble of JONSWAP initial data) is based on the inverse spectral theory of the NLS equation. For periodic boundary conditions $u(x + L, t) = u(x, t)$, the Floquet spectrum associated with an NLS potential u (i.e. the spectrum of the linear operator $\mathcal{L}^{(x)}$ at u) can be described in terms of the *Floquet discriminant* of u, defined as the trace of the transfer matrix of a fundamental matrix solution Φ of (2) over the interval $[0, L]$ [3]:

$$\Delta(u;\lambda) = \text{Trace}\left(\Phi(x,t;\lambda)^{-1}\Phi(x+L,t;\lambda)\right).$$

Then, the Floquet spectrum is defined as the region

$$\sigma(u) = \{\lambda \in \mathbb{C} \,|\, \Delta(u;\lambda) \in \mathbb{R}, -2 \le \Delta \le 2\}.$$

Points of the *continuous spectrum* of u are those for which the eigenvalues of the transfer matrix have unit modulus, and therefore $\Delta(u;\lambda)$ is real and between 2 and -2; in particular, the real line is part of the continuous spectrum. Points of the L-periodic/antiperiodic *discrete spectrum* of u are those for which the eigenvalues of the transfer matrix are ± 1, equivalently $\Delta(u;\lambda) = \pm 2$. Points of the discrete spectrum which are embedded in a continuous band of spectrum have to be critical points for the Floquet discriminant (i.e., $\mathrm{d}\Delta/\mathrm{d}\lambda$ must vanish at such points).

Because the transfer matrix only changes by conjugation when we shift in x or t, Δ is independent of those variables. An important consequence of this observation is that the Floquet discriminant is invariant under the NLS flow, and thus encodes an infinite family of constants of motion (parametrized by λ).

The continuous part of Floquet spectrum of a generic NLS potential consists of the real axis and of complex bands terminating in *simple points* λ_j^s (at which $\Delta = \pm 2, \Delta' \neq 0$). The *N-phase potentials* are those characterized by a finite number of bands of continuous spectrum (or a finite number of simple points). Fig. 2 shows the spectrum of a typical N-phase potential: complex critical points (usually *double points* of the discrete spectrum for which $\Delta' = 0$ and $\Delta" \neq 0$), such as the one appearing in the figure, are in general associated with linear instabilities of u and label its homoclinic orbits [11]. Fig. 8a shows spectrum of an N-phase potential near the one shown in Fig. 2: the complex double point has split into a pair of simple points; such a potential possesses no linear unstable modes (simple points and real double points are in general associated with neutrally stable modes).

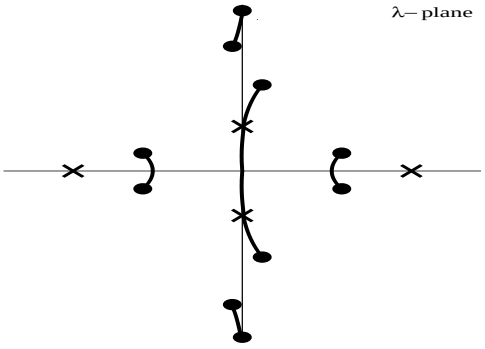

Fig. 2. Spectrum of an unstable N-phase solution. The simple periodic eigenvalues are labeled by circles and the double points by crosses.

2.1 Homoclinic solutions of the NLS equation as candidates for rogue waves

Modulationally unstable solutions of the NLS equation (e. g. N-phase solutions whose Floquet spectra have complex double points) have homoclinic orbits that can undergo large amplitude excursions away from their target solution. Such homoclinic orbits can be used as models of rogue waves.

An important (and the simplest) example of unstable NLS solution is the *plane* (or *Stokes*) *wave* potential

$$u_a(x,t) = ae^{2ia^2t}. \tag{3}$$

Elementary Fourier analysis shows that the plane wave is unstable when its amplitude a is sufficiently large: in fact, for $0 < \pi n/L < a$, the solution of the linearized NLS equation about u_a has M linearly unstable modes (UMs) $e^{\sigma_n t + 2\pi n x/L}$ with growth rates σ_n given by

$$\sigma_n^2 = \mu_n^2(\mu_n^2 - 4a^2), \quad \mu_n = 2\pi n/L,$$

where M is the largest integer satisfying $0 < M < aL/\pi$.

One can also check (see e. g. [9]) that for $0 < \pi n/L < 0$ the Floquet spectrum of the plane wave potential u_a has exactly M complex double points, each "labelling" an associated unstable mode.

Using Bäcklund transformations [26, 25] one can in principle construct the family of homoclinic orbits of an unstable NLS potential. In fact, this method gives explicit formulas for homoclinic orbits of N-phase solutions, although their expressions become rather complicated for $N > 2$. For NLS potentials with several unstable modes, iterated Bäcklund transformations will generate their entire stable and unstable manifolds, comprised of homoclinic orbits of increasing dimension up to the dimension of the invariant manifolds. Such higher-dimensional homoclinic orbits associated with two or more UMs are also known as *combination* homoclinic orbits.

A single (i. e. lowest dimensional) homoclinic orbit of the plane wave potential is given by

$$u(x,t) = ae^{-2ia^2t}\,\frac{1 + 2\cos(px)e^{\sigma_n t + 2i\phi + \rho} + Ae^{2\sigma_n t + 4i\phi + 2\rho}}{1 + 2\cos(px)e^{\sigma_1 t + \rho} + Ae^{2\sigma_n t + 2\rho}} \tag{4}$$

where $A = 1/\cos^2\phi$, $\sigma_n = \pm p\sqrt{4a^2 - p^2}$, $\phi = \sin^{-1}(p/2a)$, and $p = \mu_n = 2\pi n/L < a$ for some integer n. Each UM has an associated homoclinic orbit characterized by the mode $p = \mu_n$.

Fig. 3 shows the space-time plot of the amplitude $|u(x,t)|$ of a homoclinic orbit with one UM, for $a = 0.5$, $L = 2\sqrt{2}$ and $p = 2\pi/L$. As $t \to \pm\infty$, solution (4) limits to the plane wave potential; in fact, the plane wave behavior dominates the dynamics of the homoclinic solution for most of its lifetime. As t approaches $t_0 = 0$, nonlinear focusing occurs due to the BF instability and

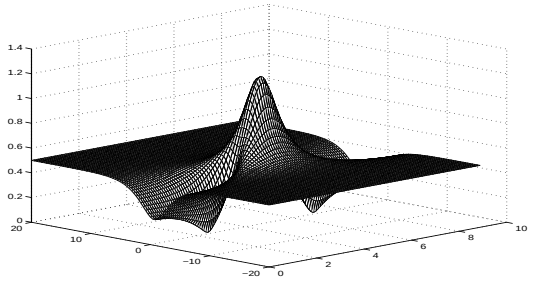

Fig. 3. Analytical rogue wave solution of the NLS corresponding to one UM.

the solution rises to a maximum height of $2.4a$. Thus, the homoclinic solution with one UM can be regarded as the simplest model of rogue wave.

An almost equally dramatic wave trough occurs close to the crest of the rogue wave as a result of wave compression due to wave dislocation. The amplitude amplification factor is given by

$$f = \frac{\max_{x\in[0,L],\, t\in\mathbb{R}}|u(x,t)|}{\lim_{t\to\pm\infty}|u(x,t)|} \approx 2.4. \tag{5}$$

In general, f depends upon the wavenumber of the modulation. As the wave number decreases, the amplification factor increases to the limiting value

$$f_{max} = \lim_{\kappa\to 0^+} f(\kappa) = 3, \tag{6}$$

although the waves take longer to reach their maximum height since their growth rate is smaller [4].

2.2 Phase modulated rogue waves

As the number of UMs increases, the space-time structure of the homoclinic solutions becomes more complex. When two or more UMs are present the initial wave train can be phase modulated to produce additional focusing.

The family of homoclinic orbits of the plane wave potential with two UMs is given by an expression of the form

$$u(x,t) = ae^{2ia^2t}\frac{g(x,t)}{f(x,t)}, \tag{7}$$

where the expression for $f(x,t)$ and $g(x,t)$ depend on the two spatial modes $\cos(2n\pi x/L)$, $\cos(2m\pi x/L)$, and on temporal exponential factors $\exp(\sigma_n t + \rho_n)$, $\exp(\sigma_m t + \rho_m)$, with growth rates $\sigma_l = \mu_l\sqrt{\mu_l^2 - 4a^2}$, $\mu_l = 2\pi l/L$. (The complete formulas can be found in [7, 9].)

As in the one-UM case, this combination homoclinic orbit decays to the plane wave potential as $t \to \pm\infty$, and the associated rogue wave remains hidden beneath the background plane wave for most of its lifetime. The temporal

separation of the two spatial modes depends upon a parameter ρ related to the difference $\rho_n - \rho_m$ in the temporal phases [7, 9].

In turn, ρ affects the amplitude amplification factor. Figs. 4a-b show the combination homoclinic orbit (7) obtained with all parameters set equal except for ρ. In Fig. 4a, $\rho = .1$, the modes are well separated, and the amplitude amplification factor is roughly three. In Fig. 4b, the value of ρ is approximately -0.65, corresponding to the two UMs being simultaneously excited or coalesced. At such ρ-value the amplitude amplification factor is maximal and the rogue wave rises to a height of 4.1 times the height of the carrier wave (whose maximum height is 2.1).

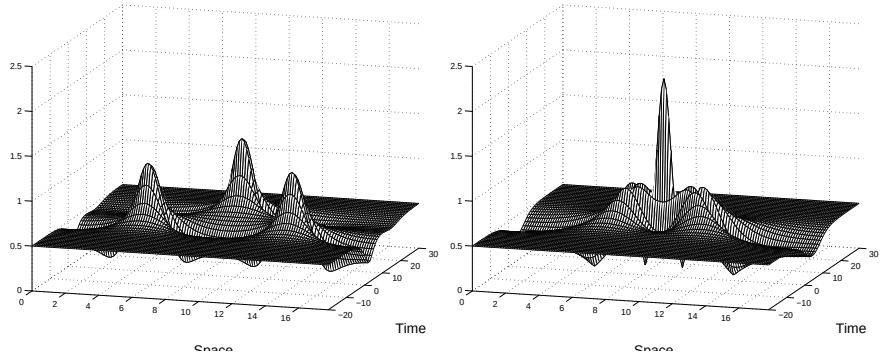

(a) (b)

Fig. 4. Rogue wave solutions of the NLS corresponding to two unstable modes (a) without phase modulation ($\rho = -1$) and (b) with phase modulation ($\rho = -0.65$).

Note that Fig. 4a shows focusing due to only weak amplitude modulation of the initial wave train; the growth in amplitude beginning at $t \approx -5$ and at $t \approx 10$ is due to the BF instability. However, in Fig. 4b focusing due to both amplitude and phase modulation occurs. The amplitude growth at $t \approx -5$ is due to the BF instability, while the additional very rapid focusing at $t \approx 3.4$ is due to the phase modulation. In general it is possible to select the phases in a combination homoclinic orbit with N spatial modes so that any number n ($2 \leq n \leq N$) of modes coalesce at some fixed time.

3 Noisy rogue waves

The Broad Bandwidth Modified NLS equation was introduced by Trulsen and Dysthe [32] as a higher order asymptotic approximation of slowly modulated periodic wave trains in deep water, assuming that the wave slope ka (where k is the wave number, and a the size of the initial displacement) is $\mathcal{O}(\epsilon)$, while the bandwidth $|\Delta k|/k$ and the quantity $(kh)^{-1}$ (where h is the water depth)

are $\mathcal{O}(\epsilon^{1/2})$. The resulting Modified Dysthe (MD) equation

$$iu_t + u_{xx} + 2|u|^2u + i\epsilon^{1/2}\left(\frac{1}{2}u_{xxx} - 6|u|^2u_x + u^2u_x^* - 2ui\left[H\left(|u|^2\right)\right]_x\right) + \\ + \epsilon\,\frac{5}{16}u_{4x} + i\epsilon^{3/2}\,\frac{7}{32}u_{5x} = 0, \tag{8}$$

is the starting point of our numerical experiments, aimed at investigating the robustness of homoclinic solutions of the NLS equation, as well as the likelihood of rogue wave generation, when higher order terms are introduced in the wave dynamics.

We choose initial data for solutions with two and three UMs; for example, in the two-UM regime, the initial condition has the form

$$u(x,0) = a\left[1 + 4i\left(\epsilon_1 \sin\phi_1 e^{i\phi_1}\cos(\frac{2\pi x}{L}) + \epsilon_2 \sin\phi_2 e^{i\phi_2}\cos(\frac{4\pi x}{L})\right)\right],$$

where the parameters ϕ_i's are varied to explore a neighborhood of the unstable plane wave potential.

Fig. 5a illustrates a striking rogue wave solution of equation (8) for $\epsilon_1 = 10^{-4}$ and $\epsilon_2 = 10^{-5}$. The solution rapidly becomes chaotic (around $t = 31$) and exhibits an irregular dynamics for a long time afterwards. At $t \approx 471.2$ a rogue wave rises from the plane wave state, developing a crest of amplitude approximately equal to four times the background wave height. The structure of this rogue wave is remarkably similar to that of the combination homoclinic solution (7) with coalesced spatial modes obtained when $\rho = -0.65$. (Compare Fig. 5a with Fig. 4b.)

Numerical simulations of the MD equation in the three-UM regime show a similar phenomenon: after the onset of chaotic dynamics, rogue waves rise intermittently above the chaotic background (see Fig. 5b). At $t \approx 208$ a rogue wave develops with a wave amplitude amplification factor of almost five. Again, the emerging rogue wave is close to the optimally phase modulated NLS homoclinic solution in the three-UM regime.

Extensive numerical experiments were performed for both the full MD model and its restriction to spatially even potentials (see Section 4) in the two- and three-UM regime, varying both perturbation strength ϵ and the values of the parameters ϕ_i's in the initial data. In all cases, the coalesced homoclinic NLS solution emerges generically as a structurally stable feature of the perturbed dynamics.

We observe how the chaotic regime produces additional focusing by effectively selecting optimal phase modulation, and how the chaotic dynamics singles out the maximally coalesced homoclinic solutions of the unperturbed NLS equation as physically observable rogue waves. Moreover, (see e. g. Fig. 5) larger amplitude waves, and more of them, are obtained for the MD equation, as also supported by the diagnostics developed in section 5, correlating wave strengths in the NLS and MD models to proximity to homoclinic data. Thus,

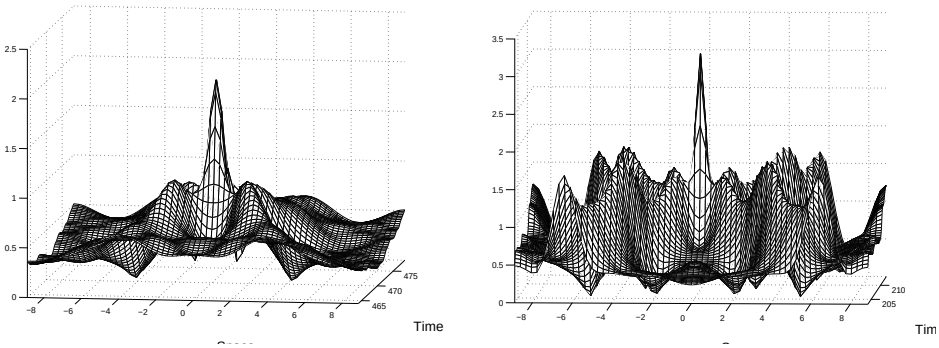

(a) (b)

Fig. 5. Rogue waves solutions for the even MD equation when (a) two and (b) three unstable modes are present.

the underlying chaotic dynamics of the MD equation appears to increase the likelihood of rogue wave generation and to favor occurrence of large amplitude rogue waves, as compared to predictions obtained from the NLS equation.

4 Melnikov Analysis

In order to better understand the emergence of the coalesced homoclinic orbit in the chaotic dynamics described by the MD equation, we use perturbation methods to construct appropriate measurements of the splitting distance of the stable and unstable manifolds of a plane wave solution with two unstable modes. In this section we briefly describe the main ingredients of the ensuing Melnikov analysis; the reader is referred to [9] for full details.

We consider the following restriction of the MD equation to spatially even potentials $u(x,t) = u(-x,t)$:

$$iu_t + u_{xx} + 2|u|^2 u = \epsilon u_{xxxx}. \tag{9}$$

Equation (9) can be regarded as a Hamiltonian dynamical system on an appropriate Sobolev space of even, periodic functions, with Hamiltonian functional $H_\epsilon(u) = \displaystyle\int_0^L (|u_x| - |u|^4 - \epsilon|u_{xx}|^2)\, dx$, and an additional conserved functional given by the L^2-norm $I(u) = \displaystyle\int_0^L |u|^2\, dx$.

For $\epsilon = 0$, we consider a plane wave potential u_a with two UMs (equivalently, with two complex double points): linear analysis shows that u_a possesses two-dimensional stable and unstable eigenspaces and an infinite number of center modes (characterized by complex conjugate pairs of imaginary eigenvalues). Its center-stable and center-unstable invariant manifolds coincide and

have codimension two. (In fact, they are explicitly parametrized in terms of the homoclinic solution (7).)

When $\epsilon \neq 0$, the plane wave potential persists as a solution of the perturbed equation, and its perturbed center-stable and center-unstable manifolds generically split. In finite-dimensional situations, invariant manifolds of unstable solutions can split under perturbation and intersect transversally. Such transversal intersections are often associated with chaotic behavior and with persistence of homoclinic orbits in the perturbed system. For PDEs the analogous situation is far more subtle, and rigorous analysis has been performed only in a handful of cases [12, 23, 21, 38, 39].

If we assume that the perturbed invariant manifolds split transversally, we need two independent measurements for their splitting distance (one for each direction transversal to the unperturbed invariant manifold). However, the perturbation is Hamiltonian, so the splitting occurs within the codimension one energy surface $H_\epsilon = const$, thus reducing the number of measurements to one.

In order to define suitable measurements, we recall how the Floquet discriminant $\Delta(u;\lambda)$ of an NLS solution u, viewed as a functional on the NLS phase space, encodes an infinite family of constants of motion [22]. Given a solution u_c with a purely imaginary critical point λ^c (such as, for example, an unstable plane wave potential), regarding λ^c as a functional on a neighborhood $\mathcal{U}$ of u_c, the functional $F : \mathcal{U} \to \mathbb{C}$,

$$\boldsymbol{F}(u) := \Delta(\lambda^c(u); u), \tag{10}$$

is locally smooth, provided $\dfrac{d^2\Delta}{d\lambda^2}(\lambda, u) \neq 0$, $\forall\, u \in \mathcal{U}$. Then, the sequence

$$F_j(u) = \Delta(\lambda_j^c(u), u),$$

generated as λ_j^c varies among the critical points of the potential u, defines a natural family of constants of motion, which identify the critical level sets of u by labelling them in terms of the double points of its Floquet spectrum.

One of the main advantages of this representation of the constants of motion of the NLS equation is that the gradient of F_j can be explicitly expressed in terms of solutions of the AKNS system by means of the following remarkable formula [22]:

$$\frac{\delta F_j}{\delta \mathbf{u}}(u) = i\frac{\sqrt{\Delta^2 - 4}}{W[\boldsymbol{\psi}^+, \boldsymbol{\psi}^-]} \left[\begin{array}{c} \psi_2^+\psi_2^- \\ -\psi_1^+\psi_1^- \end{array} \right]\Bigg|_{\lambda=\lambda^c}. \tag{11}$$

In formula (11), $\mathbf{u} = (u, u^*)$, $\boldsymbol{\psi}^\pm(x,\lambda)$ are the Bloch eigenfunctions (common eigenfunctions of the operator $\mathcal{L}^{(x)}$ and the shift operator $(\mathcal{S}\psi)(x) = \psi(x+L)$), and W denotes the Wronskian.

We observe that $\delta F_j/\delta \mathbf{u}$ vanishes at a critical potential u_c (such as the plane wave solution), reflecting the fact that F_j is critical along the critical level set. On the other hand, if u_h is a homoclinic orbit of u_c, then

$\delta F_j/\delta \mathbf{u}(u_h) \neq 0$; therefore $\delta F_j/\delta \mathbf{u}\,(u^h)$, $j = 1, \ldots M$, (M being the number of complex double points in the spectrum of u_c) define directions transversal to the homoclinic manifold.

Returning to the even restriction of the MD equation (9), the components of the splitting distance of the perturbed stable and unstable manifolds of a plane wave potential with two UMs along directions ∇F_j, $j = 1, 2$ are expressed in terms of the following Melnikov-type integrals:

$$d_j = \epsilon M_j(\rho) + \mathcal{O}(\epsilon^2), \qquad M_j(\rho) = \int_{-\infty}^{+\infty} \langle \nabla F_j, f \rangle|_{u=u_h}\, dt, \tag{12}$$

where $f(\mathbf{u}) = (u_{xxxx}, u^*_{xxxx})$ is the vector of the perturbation, $<\ ,\ >$ is the standard inner product in $L^2([0, L], \mathbb{C})$, and u_h is the homoclinic orbit (7). Both measurements depend on parameter ρ, the same parameter that governs the temporal separation of the spatial modes of the unperturbed homoclinic orbit (7) (see Section 2.2).

Consistent with the dimensional count for the splitting distance, numerical evaluation of the two Melnikov integrals show that M_1 and M_2 are mutually proportional functions of the parameter ρ (i. e. a single measurement is sufficient). Fig. 6 shows existence of a unique nondegenerate zero of M_1, suggesting that a transversal homoclinic structure persists under perturbation.

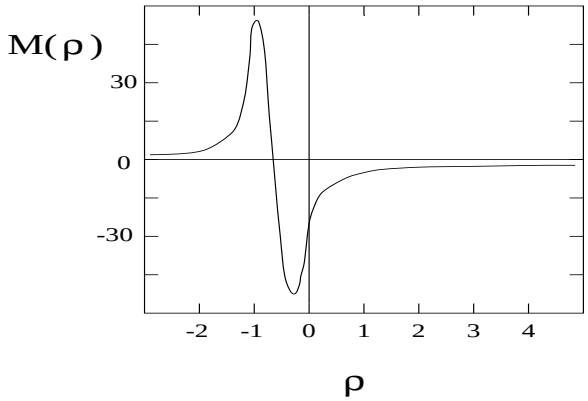

Fig. 6. Graph of the Melnikov integral M_1 as a function of parameter ρ. A transversal zero occurs at $\rho = -0.65$.

A truly remarkable fact, is that the nondegenerate zero of $M_1(\rho)$ coincides (up to order ϵ) with the value of ρ at which the two spatial modes of the homoclinic solution (7) coalesce, producing a homoclinic orbit of maximal amplitude. The same structure is observed as the recurring structurally stable feature of the chaotic dynamics. (See Fig. 5.)

A study of the analytical structure of single and combination homoclinic orbits, together with the numerical experiments and the Melnikov analysis, supports the following:

–Although homoclinic solutions of the NLS equation have many of the features of rogue waves, not all can be regarded as good candidates for modelling actual rogue waves, as not all are robust under perturbations that lead to more accurate physical models.

–For sea states characterized by a finite number of unstable modes, the homoclinic solutions that are robust under perturbation are the combination homoclinic orbits: 1) with a maximal number of spatial modes excited (this should not be a surprise, since the lower-dimensional homoclinic solutions are linear unstable); and 2) for which the spatial modes are optimally coalesced.

–A chaotic sea state enhances the occurrence of rogue waves. One should note that a homoclinic solution of the NLS will rise over the background wave only once in its life time and for a relative brief time. However, in a chaotic evolution, the maximally coalesced homoclinic orbit will occur repeatedly, although in an unpredictable fashion.

5 Random oceanic sea states and the proximity to homoclinic data

To study the generation of rogue waves in a random sea state, we consider initial data for the surface elevation to be of the form [29]

$$\eta(x,0) = \sum_{n=1}^{N} C_n \cos\left(k_n x - \phi_n\right), \tag{13}$$

where $k_n = 2\pi n/L$ and the random phases ϕ_n are uniformly distributed on $(0, 2\pi)$ and the spectral amplitudes, $C_n = \sqrt{2S(f_n)/L}$, are obtained from the JONSWAP spectrum [27]:

$$S(f) = \frac{\alpha g^2}{(2\pi f)^5} \exp\left[-\frac{5}{4}\left(\frac{f_0}{f}\right)^4\right] \gamma^r, \qquad r = \exp\left[-\frac{1}{2}\left(\frac{f-f_0}{\sigma_0 f_0}\right)^2\right]. \tag{14}$$

Here f is spatial frequency, $f_n = k_n/2\pi$, f_0 is the dominant frequency, determined by the wind speed at a specified height above the sea surface, g is gravity, and $\sigma_0 = 0.07$ (0.9) for $f \leq f_0$ ($f > f_0$). In contrast to physical experiments, which monitor the surface evolution at a given spatial point (probe) in time, here we take time slices and examine the features in space.

JONSWAP spectra describe developing sea states since for $\gamma > 1$ the wave spectra continues to evolve through nonlinear wave-wave interactions for very long times and distances. As γ is increased, the spectrum becomes narrower

about the dominant peak (see Fig. 6). In this sense, γ is considered the "peak-shape" parameter.

The scale parameter α is related to the amplitude and energy content of the wavefield. Based on an "Ursell number", the ratio of the nonlinear and dispersive terms of the NLS equation (1) in dimensional form, the NLS equation is considered to be applicable for $2 < \gamma < 8$ [29]. Typical values of alpha are $0.008 < \alpha < 0.02$.

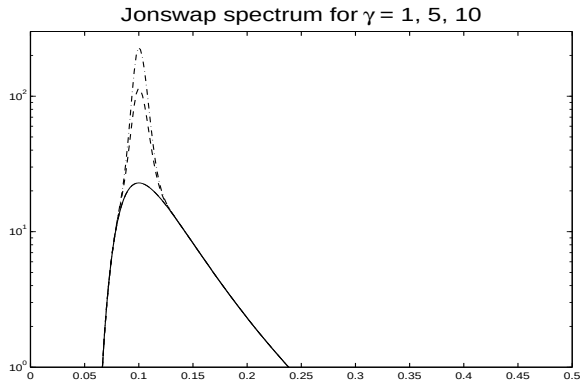

Fig. 7. The JONSWAP spectrum for $\gamma = 1$ (solid line), $\gamma = 5$ (dashed line), and $\gamma = 10$ (dash-dot line) with $f_0 = 0.1$ Hz and $\alpha = 0.0081$.

In the numerical experiments, the NLS and MD equations are integrated using a pseudo-spectral scheme with 256 Fourier modes in space and a fourth order Runge-Kutta discretization in time ($\Delta t = 10^{-3}$). The nonlinear mode content of the data is numerically computed using the direct spectral transform described above, i.e. the system of ODEs (2) is numerically solved to obtain the discriminant Δ. The zeros of $\Delta \pm 2$ are then determined with a root solver based on Muller's method [11]. The spectrum is computed with an accuracy of $\mathcal{O}(10^{-6})$, whereas the spectral quantities we are interested in range from $\mathcal{O}(10^{-2})$ to $\mathcal{O}(10^{-1})$.

Under perturbation complex double points typically split into two simple points, $\lambda_\pm$, thus opening a gap in the band of spectrum (see Fig. 2). We refer to the distance between these two simple points, $\delta(\lambda_+, \lambda_-) = |\lambda_+ - \lambda_-|$, as the splitting distance. As mentioned, homoclinic solutions arise as an appropriate degeneration of a finite gap solution [15], i.e. when the resulting double point, $\delta(\lambda_+, \lambda_-) \to 0$, is complex. Consequently, we can use δ to measure the proximity in the spectral plane to homoclinic data, i.e. to complex double points and their corresponding instabilities. Since the NLS spectrum is symmetric with respect to the real axis and real double points correspond to inactive modes, in subsequent plots only the spectrum in the upper half complex λ-plane will be displayed.

Our first step is to determine the spectrum of JONSWAP initial data given by (13) for various combinations of $\alpha = .008, .012, .016, .02$, and $\gamma = 1, 2, 4, 6, 8$. For each such pair (γ, α), we performed fifty simulations, each with a different set of randomly generated phases. As expected, the spectral configuration depends on the energy α and the enhancement coefficient γ. However, the extent of the dependence of features of the spectrum, such as the proximity to complex double points, upon the phases in the initial data is surprising.

Typical examples of the results are given in Figs. 8a and 8b which show the numerically computed nonlinear spectrum of JONSWAP initial data when $\gamma = 4$ and $\alpha = .016$ for two different realizations of the random phases.

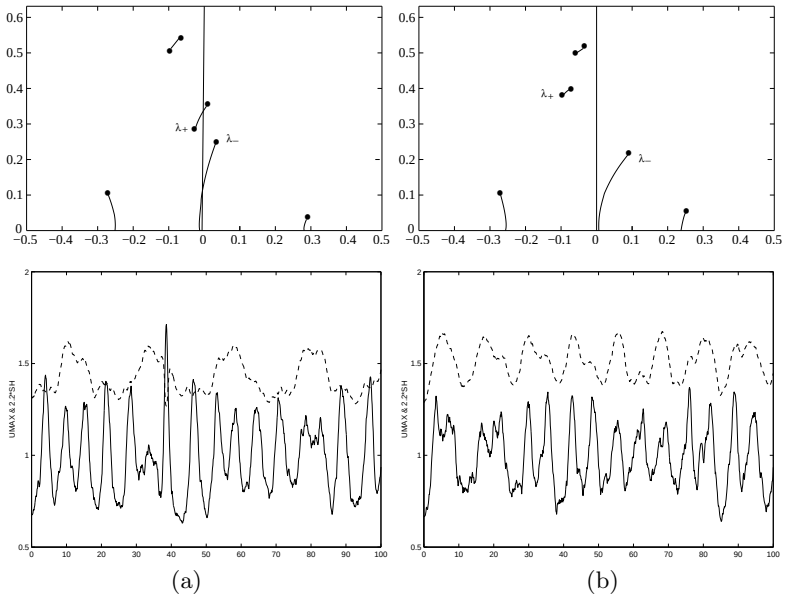

Fig. 8. Spectrum and evolution of U_{max} (a) "near" and (b) "far" from homoclinic data.

We find that JONSWAP data correspond to "semi-stable" N-phase solutions, i.e. JONSWAP data can be viewed as perturbations of N-phase solutions with one or more unstable modes (compare Fig. 2 with the spectrum of an unstable N-phase solution in Fig. 8). In Fig. 8a the splitting distance $\delta(\lambda_+, \lambda_-) \approx .07$, while in Fig. 8b $\delta(\lambda_+, \lambda_-) \approx .2$. Thus the JONSWAP data can be quite "near" homoclinic data as in Fig. 8a or "far" from homoclinic data as in Fig. 8b, depending on the values of the phases ϕ_n in the initial data. For all the examined values of α and γ we find that, when α and γ are fixed, as the phases in the JONSWAP data are varied, the spectral distance δ of typical JONSWAP data from homoclinic data varies.

Most importantly, irrespective of the values of the JONSWAP parameters α and γ, in simulations of the NLS equation (1) we find that extreme waves develop for JONSWAP initial data that is "near" NLS homoclinic data, whereas the JONSWAP data that is "far" from NLS homoclinic data typically does not generate extreme waves. Figs. 8c and 8d show the corresponding evolution of the maximum surface elevation, U_{max}, obtained with the NLS equation. U_{max} is given by the solid curve and as a reference, $2.2H_S$ (the threshold for a rogue wave) is given by the dashed curve. H_S is the significant wave height and is calculated as four times the standard deviation of the surface elevation. Fig. 8c shows that when the nonlinear spectrum is near homoclinic data, U_{max} exceeds $2.2H_S$ (a rogue wave develops at $t \approx 40$). Fig. 8d shows that when the nonlinear spectrum is far from homoclinic data, U_{max} is significantly below $2.2H_S$ and a rogue wave does not develop. As a result we can correlate the occurrence of rogue waves characterized by JONSWAP spectrum with the proximity to homoclinic solutions of the NLS equation.

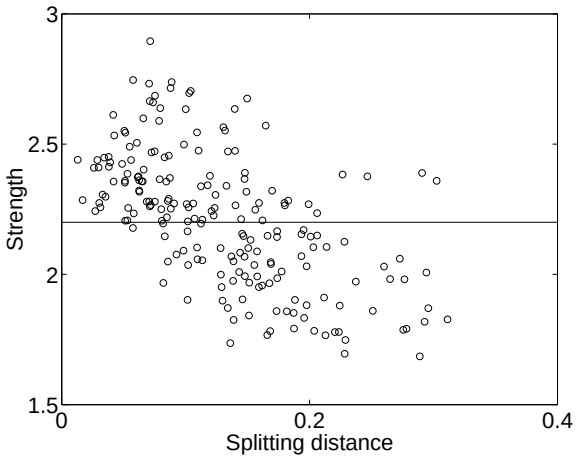

Fig. 9. Strength of U_{max}/H_s vs. the splitting distance $\delta(\lambda_+, \lambda_-)$ for solutions of the NLS equation.

The results of hundreds of simulations of the NLS and MD equations consistently show that proximity to homoclinic data is a crucial indicator of rogue wave events. Fig. 9 and 10 provide a synthesis of 200 random simulations of the NLS equation and of the MD equation for two perturbation strengths ($\epsilon = 0.005$ and $\epsilon = 0.01$) for JONSWAP initial data with different (γ, α) pairs (with $\gamma = 2, 4, 6, 8$, and $\alpha = .012, .016$). For each such pair (γ, α), we performed 25 simulations, each with a different set of randomly generated phases. We restrict our consideration to semi-stable N-phase solutions near to unstable solutions of the NLS with one UM. Each circle represents the strength of the maximum wave (U_{max}/H_S) attained during one simulation as

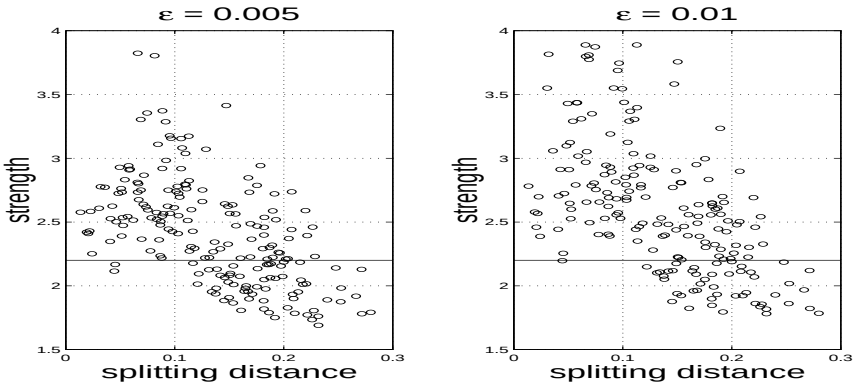

Fig. 10. Strength of U_{max}/H_s vs. the splitting distance $\delta(\lambda_+, \lambda_-)$ for solutions of the MD equation when (a) $\epsilon = .005$ and (b) $\epsilon = .01$.

a function of the splitting distance $\delta(\lambda_+, \lambda_-)$. The results for the particular pair $(\gamma = 4, \alpha = 0.012)$ is represented with an asterisk. A horizontal line at $U_{max}/H_S = 2.2$ indicates the reference strength for rogue wave formation. We identify two critical values $\delta_1(\epsilon)$ and $\delta_2(\epsilon)$ that clearly show that (a) if $\delta < \delta_1$ (near homoclinic data) rogue waves will occur; (b) if $\delta_1 < \delta < \delta_2$, the likelihood of obtaining rogue waves decreases as δ increases and, (c) if $\delta > \delta_2$ the likelihood of a rogue wave occurring is extremely small.

This behavior is robust. As α and γ are varied, the strength of the maximum wave and the occurrence of rogue waves are well predicted by the proximity to homoclinic solutions. The individual plots of the strength vs. δ for particular pairs (γ, α) are qualitatively the same regardless of the pair chosen. As noted in section 4 on the MD equation, enhanced focusing occurs in the chaotic regime. Fig. 10 shows that as ϵ increases the average strength and the likelihood of rogue waves increases. Clarification on the likelihood of rogue waves through an examination of the kurtosis is provided in the next section. These results give strong evidence of the relevance of homoclinic solutions of the NLS equation in investigating rogue wave phenomena for more realistic oceanic conditions and identifies the nonlinear spectral decomposition as a simple diagnostic tool for predicting the occurrence and strength of rogue waves.

6 Non-Gaussian statistics and the dependence of kurtosis on the proximity to homoclinic data

In [24] the probability distribution of crest-to-trough wave heights was formulated to be given by the Rayleigh distribution when the wave spectrum is narrow banded and the phases in the reconstruction of the surface elevation

are uniformly distributed. Various studies using experimental and field wave data have shown that this can be a reasonable assumption for water waves in the linear regime.

In the nonlinear regime, the relation of the probability density function of wave heights to the nonlinear parameters describing various sea states is not generally known. Simply assuming a Gaussian distribution can be risky. If the kurtosis is in fact much greater than that for the Gaussian distribution, then the probability of an extreme event will be underpredicted.

The main questions we address in this section are whether the modulational instability and the presence of coherent structures yield non-Gaussian statistics of surface gravity waves in the nonlinear regime and whether this can be captured by the spectral parameter δ. In our earlier work with the NLS equation it appeared that homoclinic chaos increases the likelihood of rogue waves. After a short time the waves become chaotic resulting in a sea state characterized by intermittent rogue waves. To more precisely quantify rogue wave events, in our current numerical experiments we monitor the evolution of the skewness, m_3, and the kurtosis, m_4, of the wavefield which are related to the third and fourth statistical moments of the probability density function of the surface elevation by

$$m_3(\eta) = \sum_{j=1}^{N} \frac{(\eta_j - \bar{\eta})^3}{N\sigma^3}, \qquad m_4(\eta) = \sum_{j=1}^{N} \frac{(\eta_j - \bar{\eta})^4}{N\sigma^4},$$

where σ is the standard deviation of the surface elevation, $\bar{\eta}$ is the average surface elevation and N is the number of data points sampled.

Skewness is a measure of the vertical asymmetry of the wavefield. Positive values indicate the wavefield is skewed above average height, i.e. the crests are bigger than the troughs. Negative values indicate that the wavefield is skewed below average height.

The kurtosis is a measure of whether the distribution for the wavefield is peaked or flat, relative to a Gaussian distribution and defines the contribution of large waves to the wavefield. The kurtosis for a Gaussian distribution is three. Wavefields with high kurtosis (in excess of 3) tend to have a distinct peak near the mean, decline rapidly, and have heavy tails. That is, fewer observations or events cluster near the average and more observations populate the extremes either far above or far below the average compared to the bell curve of the normal distribution. For this reason, excess kurtosis much above three indicates that the contribution of large waves is significant and corresponds to a higher probability of a rogue wave event.

Fig. 11 (a) shows the plot of the kurtosis as a function of time for the analytical two unstable mode homoclinic solutions of the NLS (7) (the corresponding waveforms are given in Fig. 4) in the uncoalesced case, $\rho = -1$, and in the coalesced case, $\rho = -0.65$. Here we are using the kurtosis as a formal tool to obtain a rough estimate of the peakedness of the waveform. In both cases the kurtosis starts to increase with the onset of the BF instability and

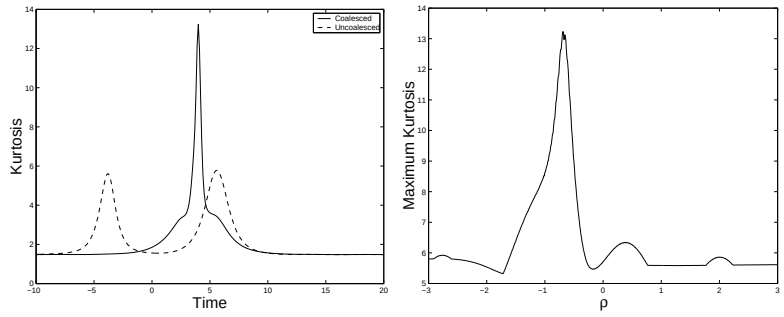

(a) (b)

Fig. 11. For the two unstable mode homoclinic solution of NLS: (a) the evolution of the kurtosis for the coalesced and uncoalesced cases and (b) the maximum of the kurtosis as a function of ρ.

reaches a maximum when the instability saturates. In the uncoalesced case there are two excursions in the kurtosis. In the coalesced case, the increased height achieved by the waveform is reflected in a significantly larger kurtosis. Fig. 11(b) shows the plot of the maximum of the kurtosis of the two unstable mode homoclinic orbit, as a function of the phase parameter ρ. Interestingly, the maximum of the kurtosis is optimized by the robust coalesced homoclinic solution which also gives the zero of the Melnikov integrals and is persistent in the MD equation.

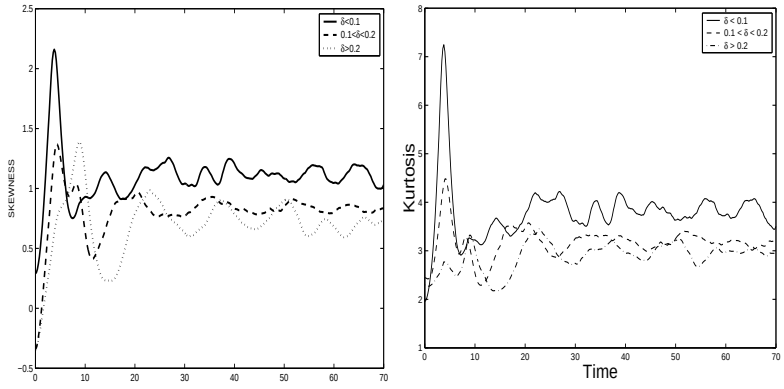

(a) (b)

Fig. 12. Evolution of the (a) skewness and (b) kurtosis for Jonswap initial data.

In [16] Janssen formulated the relation between the kurtosis of the surface elevation and the probability of rogue wave occurrence for $1D$ weakly non-Gaussian waves. A is the envelope of the wavetrain and ϕ the phase. The

PDF of the envelope A follows from an integration of the joint probability distribution over the phase ϕ. The first term gives the Rayleigh distribution while the terms involving the skewness integrate to zero. The third term does give a contribution depending on the kurtosis and they find that the narrow-band approximation of the PDF of the envelope is

$$p(A) = Ae^{-\frac{1}{2}A^2}\left[1 + \frac{1}{3}m_4\left(1 - A^2 + \frac{1}{8}A^4\right)\right].$$

The probability of the occurrence of a rogue wave as a function of N (the number of waves) and the kurtosis is

$$\mathcal{P}_{rogue} = 1 - \exp\left[-e^{-8}N\left(1 + 8m_4\right)\right].$$

In this way, as the kurtosis increases, the probability that rogue waves will occur increases. We examine the evolution of the skewness and kurtosis for three ranges of δ: i) $\delta \leq .1$, ii) $.1 < \delta < .2$, and iii) $\delta \geq .2$. The skewness and kurtosis is computed at each time step, first as an average over space and then averaging over the ensemble. As before, we begin by determining the nonlinear spectrum of the JONSWAP initial data for various combinations of (α, γ). We used a sufficient number of realizations of the random phases so that we would have 250 cases for each range of values of δ. Fig. 12 provides the evolution of the skewness and kurtosis for three different values of the nonlinear spectral gap size δ. Both the skewness and kurtosis grows initially and then relax to their asymptotic value. The asymptotic value of the kurtosis is approximately i) 3.5 when $\delta \leq .1$, ii) 3.2 when $.1 < \delta < .2$, and iii) 3 when $\delta \geq .2$. It is clear in Fig. 12 the kurtosis is strongly dependent on δ and attains larger values for Jonswap data closer to homoclinic data. The proximity to homoclinic data changes the wave statistics and increases the likelihood of rogue waves.

Using the inverse spectral theory of the NLS equation, we have shown that the development of extreme waves in random oceanic sea states characterized by JONSWAP power spectra is well predicted by the proximity to homoclinic data of the NLS equation. We observe that the modulational instability generates a significant deviation from Gaussianity. In particular we find: i) the kurtosis and wave strength are found to be strongly dependent on δ, the proximity to instabilities and homoclinic structures; ii) the likelihood of rogue waves increases for JONSWAP data near to homoclinic data of the NLS; iii) the NLS equation underpredicts, as compared to the MD equation, both the wave strength and likelihood of rogue waves.

References

1. Ablowitz MJ, Hammack J, Henderson D, Schober CM (2000) Modulated Periodic Stokes Waves in Deep Water. Phys. Rev. Lett. 84:887–890.

2. Ablowitz MJ, Hammack J, Henderson D, Schober CM (2001) Long time dynamics of the modulational instability of deep water waves. Physica D 152-153:416–433.
3. Ablowitz MJ, Segur H (1981) Solitons and the Inverse Scattering Transform. SIAM.
4. Akhmediev NN, Korneev VI, Mitskevich NV (1988) N-modulation signals in a single-mode optical waveguide under nonlinear conditions. Sov. Phys. JETP 67:1.
5. Bridges TJ, Derks G (1999) Unstable eigenvalues and the linearization about solitary waves and fronts with symmetry. Proc. Royal Soc. London A 455:2427.
6. Cai D, McLaughlin DW, McLaughlin KTR (1995) The Nonlinear Schrödinger Equation as both a PDE and a Dynamical System. Preprint.
7. Calini A, Ercolani NM, McLaughlin DW, Schober CM (1996) Mel'nikov analysis of numerically induced chaos in the nonlinear Schrödinger equation. Physica D 89:227–260.
8. Calini A, Schober CM (2001) Chaotic dynamics for a symmetry breaking perturbation of the NLS equation. J. Math. and Comp. Sim. 55:351–364.
9. Calini A, Schober CM (2002) Homoclinic chaos increases the likelihood of rogue waves. Phys. Lett. A 298:335–349.
10. Dysthe K, Trulsen K (1999) Note on breather type solutions of the NLS as model for freak waves. Phys. Scripta T82:48–52.
11. Ercolani N, Forest MG, McLaughlin DW (1990) Geometry of the Modulational Instability Part III: Homoclinic Orbits for the Periodic Sine-Gordon Equation. Physica D 43:349–384.
12. Haller G, Wiggins S (1992) Orbits homoclinic to resonances: the Hamiltonian case. Physica D 66:298–346.
13. Henderson KL, Peregrine DH, Dold JW (1999) Unsteady water wave modulations: fully nonlinear solutions and comparison with the nonlinear Schrödinger equation. Wave Motion 29:341.
14. Islas A, Schober CM (2005) Predicting rogue waves in random oceanic sea states. Phys. Fluids 17:1–4.
15. Its AR, Salle MA, Rybin AV (1988). Teor. Mat. Fiz 74:29–45.
16. Janssen P (2003) Nonlinear four-wave interactions and freak waves. Jour. Phys. Oceanography 33:863–884.
17. Karjanto N (2006) Mathematical Aspects of Extreme Water Waves. Ph.D. Thesis, Universiteet Twente.
18. Kharif C, Pelinovsky E (2004) Physical mechanisms of the rogue wave phenomenon. Eur. J. Mechan B/Fluids. J. Mech. 22:603–634.
19. Kharif C, Pelinovsky E (2001) Focusing of nonlinear wave groups in deep water. JETP Lett. 73: 170–175.
20. Krichever IM (1977) Methods of algebraic geometry in the theory of nonlinear equations. Russian Math. Surv. 32:185–213.
21. Li Y (1999) Homoclinic tubes in the nonlinear Schrödinger equation under Hamiltonian perturbations. Prog. Theo. Phys. 101:559-577.
22. Li Y, McLaughlin DW (1994) Morse and Mel'nikov Functions for NLS Pde's Discretized Perturbed NLS Systems. I. Homoclinic Orbits. Comm. Math. Phys. 612:175–214.
23. Li Y, McLaughlin DW, Shatah J, Wiggins S (1996) Persistent Homoclinic Orbits for a Perturbed Nonlinear Schrödinger Equation. Comm. Pure Appl. Math. 49:1175–1255.

24. Longuet-Higgins MS (1952) On the statistical distribution of the heights of sea waves. J. Mar. Res. 11:1245.
25. Matveev VB, Salle MA (1991) Darboux Transformations and Solitons. Springer-Verlag.
26. McLaughlin DW, Schober CM (1992) Chaotic and homoclinic behavior for numerical discretizations of the nonlinear Schrodinger equation. Physica D 57:447–465.
27. Ochi MK (1998) Ocean waves: the stochastic approach. Cambridge University Press.
28. Osborne A, Onorato M, Serio M (2000) The nonlinear dynamics of rogue waves and holes in deep-water gravity wave trains. Phys. Lett. A 275:386.
29. Onorato M, Osborne A, Serio M, Bertone S (2001) Freak wave in random oceanic sea states. Phys. Rev. Lett. 86:5831.
30. Schober C (2006) Melnikov analysis and inverse spectral analysis of rogue waves in deep water. Eur. J. of Mech. B - Fluids 25.
31. Torcini A, Frauenkron H, Grassberger P (1997) Studies of phase turbulence in the one-dimensional complex Ginzburg-Landau equation. Phys. Rev. E 55:5073–5081.
32. Trulsen K, Dysthe K (1996) A modified nonlinear Schrödinger equation for broader bandwidth gravity waves on deep water. Wave Motion 24:281.
33. Trulsen K, Dysthe K (1997) Frequency downshift in three-dimensional wave trains in a deep basin. J. Fluid Mech. 352:359–373.
34. Trulsen K, Dysthe K (1997) Freak waves – a three dimensional wave simulation. In: E.P. Rood (ed) Naval Hydrodynamics. Proc. 21st Sympos. Nat. Acad. Press.
35. van Groesen EWC, Karjanto N, Peterson P, Andonowati A Wave dislocation and nonlinear amplitude amplification for extreme fluid surface waves. preprint.
36. White BS, Fornberg B (1998) On the chance of freak waves at sea. J.Fluid Mech. 355:113–138.
37. Zakharov VE, Shabat AB (1972) Exact theory of two-dimensional self-focusing and one-dimensional self-modulation of waves in nonlinear media. Sov. Phys. JETP 34:62–69.
38. Zeng C (2000) Homoclinic orbits for a perturbed nonlinear Schrdinger equation. Comm. Pure Appl. Math. 53:1222–1283.
39. Zeng C (2000) Erratum: "Homoclinic orbits for a perturbed nonlinear Schrdinger equation". Comm. Pure Appl. Math. 53:1603–1605.